Laser and Particle Beams (2009), *27*, 327–333. Printed in the USA.
Copyright © 2009 Cambridge University Press 0263-0346/09 $20.00
doi:10.1017/S0263034609000433

Enhanced ion acceleration by collisionless electrostatic shock in thin foils irradiated by ultraintense laser pulse

M.-P. LIU,[1] B.-S. XIE,[1,2,3] Y.-S. HUANG,[4] J. LIU,[5] AND M.Y. YU[6,7]

[1]Key Laboratory of Beam Technology and Materials, Modification of the Ministry of Education, Beijing Normal University, Beijing, People's Republic of China
[2]College of Nuclear Science and technology, Beijing Normal University, Beijing, People's Republic of China
[3]Beijing Radiation Center, Beijing, People's Republic of China
[4]Department of Engineering Physics, Tsinghua University, Beijing, People's Republic of China
[5]Institute of Applied Physics and Computational Mathematics, Beijing, People's Republic of China
[6]Institute for Fusion Theory and Simulation, Department of Physics, Zhejiang University, Hangzhou, People's Republic of China
[7]Institut für Theoretische Physik I, Ruhr-Universität Bochum, Bochum, Germany

(RECEIVED 15 November 2008; ACCEPTED 24 February 2009)

Abstract

The formation of collisionless electrostatic shock (CES) and ion acceleration in thin foils irradiated by intense laser pulse is investigated using particle-in-cell simulation. The CES can appear in the expanding plasma behind the foil when self-induced transparency occurs. The transmitting laser pulse can expel target-interior electrons, in addition to the electrons from the front target surface. The additional hot electrons lead to an enhanced and spatially-extended sheath field behind the foil. As the CES propagates in the plasma, it also continuously forward-reflects many of the upstream ions to higher energies. The latter ions are further accelerated by the enhanced sheath field and can overtake and shield the target-normal sheath accelerated ions. The energy gain of the CES accelerated ions can thus be considerably higher than that of the latter.

Keywords: Collisionless electrostatic shock; Ion acceleration; Laser-foil acceleration; Target-normal sheath acceleration

INTRODUCTION

Energetic ions generated in intense ($I\lambda^2 > 10^{18}$ Wcm^{-2} μm^2, where I and λ are the laser intensity and wavelength, respectively) laser interaction with plasma are of much research interest because of their potential applications to fast ignition in inertial confinement fusion (Roth *et al.*, 2001; Eliezer *et al.,* 2007; Hora, 2007; Winterberg, 2008), proton radiography (Mackinnon *et al.*, 2006), radioisotope production (Santala *et al.*, 2001), etc. In the interaction, the ions in the target front surface can be accelerated against the laser pulse by the electrostatic space-charge field created by the expanding hot electrons in the front vacuum region (Nickles *et al.*, 2007; Mckenna *et al.*, 2008). On the other hand, the ions at the target rear surface are accelerated by the sheath field induced by the laser-expelled hot electrons that have passed through the target and escaped into the rear vacuum, i.e., by target-normal sheath acceleration (TNSA) (Cowan *et al.*, 2004; Roth *et al.*, 2005; Brambrink *et al.*, 2006; Limpouch *et al.*, 2008; Liu *et al.*, 2008; Huang *et al.*, 2008). In the experiments, TNSA proton bunches with energies up to 60 MeV have been reported (Snavely *et al.*, 2000). When the target thickness is comparable to the skin depth (i.e., at nanometer scale), it has been shown (Yin *et al.*, 2006; Flippo *et al.*, 2007) that ions can be accelerated violently to GeV energies by the "break-out afterburner" mechanism.

Ions can also be accelerated by collisionless electrostatic shock (CES). As a CES propagates in the plasma, the upstream ions can be continuously reflected by the shock front to high energies. The CES has been intensively investigated theoretically (Forslund & Shonk, 1970; Forslund & Freidberg, 1971; Denavit, 1992; Silva *et al.*, 2004; Chen *et al.*, 2007; He *et al.*, 2007; Sorasio *et al.*, 2006) and experimentally (Wei *et al.*, 2004; Desai *et al.*, 2007; Romagnani *et al.*, 2008; Lebo *et al.*, 2008). Recently, Silva *et al.* (2004) pointed out that in certain situations, the CES acceleration (CESA), instead of TNSA, may be responsible for the highest-energy ions found in some experiments, and has thereby motivated much interest in the CES in laser-plasma interaction. Chen *et al.* (2007) investigated the generation of CES and its structure, as well as the dependence of the CES on the laser intensity, target parameters, and preplasma. He *et al.* (2007) found that the energy spectrum of

Address correspondence and reprint requests to: Bai-Song Xie, College of Nuclear Science and technology, Beijing Normal University, Beijing 100875, People's Republic of China. E-mail: bsxie@bnu.edu.cn

https://doi.org/10.1017/S0263034609000433 Published online by Cambridge University Press

the CESA ions has a quasi-monoenergetic temporal-spatial peak and the solitary wave can only accelerate ions at the rear surface of the target. Sorasio *et al.* (2006) showed that collisions of two plasma slabs at different temperatures and densities can generate a CES with very high Mach number ($M \gg 10$). Such a fast CES can reflect and thus accelerate the ions in front of it to very high energies.

Zhidkov *et al.* (2002) found that for relatively thin overdense targets, the CESA ions in the expanding plasma can be further accelerated by the space-charge field produced by the expelled hot electrons, and form a soliton-like bunch. The velocity of the latter in the expanding plasma can exceed the maximum velocity of the TNSA ions. D'Humières *et al.* (2005) also studied the interplay between CESA and TNSA. However, the details of CES generation and the electron and ion dynamics in it are still unclear if self-induced transparency (SIT) (Lefebvre & Bonnaud, 1995) occurs. In this article, we use particle-incell (PIC) simulation to study the generation of CES in a plasma foil by an intense laser pulse and the resulting ion accelerating in the presence of SIT. The evolution of the ion momentum distribution in the generation of the CES and in the expanding plasma behind the foil is analyzed. It is shown that CES can also be formed if the plasma foil is transparent to the laser pulse, and that the resulting ion acceleration is more efficient than that by CESA in an opaque plasma, and by TNSA because of an enhanced and extended rearside sheath field.

MODEL AND SIMULATION RESULTS

We shall use a one-dimensional-3V VORPAL code (Nieter & Cray, 2004) for the PIC simulation. A laser pulse is incident normally onto the thin foil. It has a central wavelength $\lambda = 1\ \mu$m and peak intensity $I_0 = 3.5 \times 10^{20}\ \mathrm{Wcm}^{-2}$, i.e., $a_0 = eA_0 = m_e c^2 = 16$, where A_0 is the vector potential, c is the speed of light in vacuum, $-e$ and m_e are the electron charge and mass, respectively. The laser propagates along the x direction and is linearly polarized in the y direction. It has a Gaussian envelope with an full width at half maximum duration of $T_L = 100$ fs. At $t = 0$, the peak of the laser pulse is at $x = -30\ \mu$m, and it incidents on the foil surface at $t = 167$ fs. The thin foil initially occupies a region from $x = 50\ \mu$m to $x = 52\ \mu$m, its density is $n_0 = 10n_c$, where $n_c = m_e\omega^2/4\pi e^2$ is the critical plasma density, and ω is the laser frequency. The initial density is assumed to be uniform. The ion charge and mass numbers are $Z = 1$ and $M = 1$, respectively. The ion-to-electron mass ratio is $m_i/m_e = 1836$. The initial electron and ion temperatures are assumed to be small and their effects are ignored. The simulation domain spans over 100 μm. We take 550 particles per species and per cell, and the cell size is of $\lambda/200$.

When the laser pulse impinges onto the plasma foil, electrons are quickly $\mathbf{J} \times \mathbf{B}$ heated (Kruer & Estabrook, 1985) and pushed inward by the laser ponderomotive force. A strong electrostatic field at the front surface is induced, which accelerates the ions there (Badziak *et al.*, 2005). An ion-acoustic structure is excited and it propagates into the foil plasma. Furthermore, the piston-like laser field drives the ions inward into the plasma layer. The piston velocity is given by (Denavit, 1992; Silva *et al.*, 2004; Chen *et al.*, 2007)

$$\frac{v_{\mathrm{piston}}}{c} \simeq \frac{a}{\sqrt{m_i n_i}}, \tag{1}$$

where n_i is the ion density, a is the normalized vector potential, and m_i is the ion mass. The velocity v_{ias} of the electrostatic ion acoustic structure approximately equals the piston velocity v_{piston}. Thus, a sufficiently high laser intensity is required to drive the ions inward like a piston. Figure 1 shows the distribution in the ion phase space at different times. Because of hot electron recirculation (Mackinnon *et al.*, 2002; Huang *et al.*, 2007), the hot-electron temperature in the thin foil at the start of the interaction is higher than that in the thicker target. The recirculation process can not only enhance the hot electron density but also heat the other electrons in the plasma. At $t = 240$ fs, the hot-electron temperature reaches $T_e = 5.8$ MeV, which is consistent with the formula

$$T_e = 0.511\left(\sqrt{1 + a_0^2} - 1\right) = 5.3\ \mathrm{MeV}. \tag{2}$$

The piston velocity v_{piston} is about $0.0834c$. The Mach number of the ion acoustic structure is given by

$$M = \frac{v_{\mathrm{ias}}}{c_s} \simeq \frac{v_{\mathrm{piston}}}{\sqrt{Zk_B T_e/m_i}}, \tag{3}$$

where c_s is the ion acoustic speed and k_B is the Boltzmann's constant. We have $M \sim 1.057$ at $t = 240$ fs. Since M is lower than the critical Mach number $M_c = 1.6$ for CES formation, only a soliton-like ion structure is formed in the plasma foil, as shown in Figure 1a. The ions at the backside surface are effectively accelerated by TNSA and some ions at the front target surface are accelerated backwards against the laser. The peak of the laser pulse eventually reaches the turning point at about $t = 280$ fs in the plasma expansion. At $t = 295$ fs a CES is generated in the expanding plasma behind the foil as ions in the front of the electrostatic structure begin to be reflected, as shown in Figure 1b. Due to momentum conservation, the reflected ions efficiently gain energy from the CES. At about $t = 340$ fs, the CESA ions overtake the TNSA ions. Figure 1c clearly shows the formation of the CES in the expanding plasma at $t = 350$ fs. The velocity of the CES is $v_{\mathrm{shock}} = 0.2585\,c$ and the Mach number reaches about 3.2. The CESA ions can shield the TNSA ions. Figure 1d shows that the CES can accelerate ions more efficiently than TNSA. We see that at $t = 350$ fs the maximum velocities of the CESA and TNSA ions are $0.43c$ and $0.28\ c$, respectively, and at $t = 550$ fs the corresponding velocities are $0.515\ c$ and $0.32\ c$.

https://doi.org/10.1017/S0263034609000433 Published online by Cambridge University Press

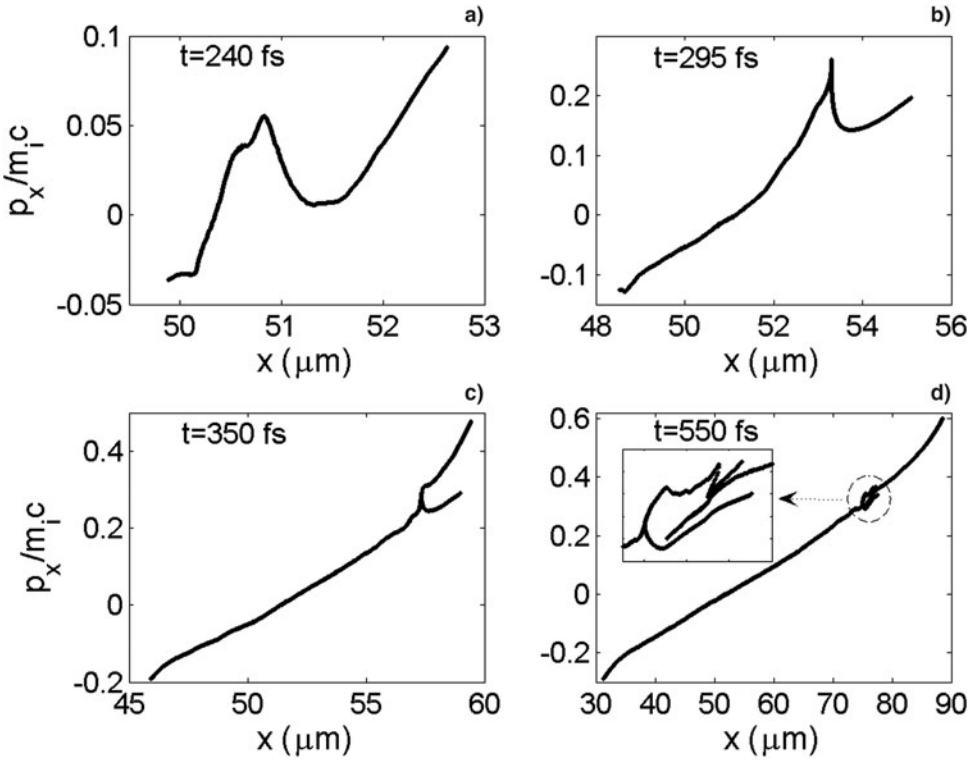

Fig. 1. Ion phase space (x, p_x) at (**a**) $t = 240$ fs, (**b**) $t = 295$ fs, (**c**) $t = 350$ fs, and (**d**) $t = 550$ fs, respectively. The foil density is $n_{e0} = 10n_c$. The peak intensity and pulse duration of the laser pulse are $a_0 = 16$ and 100 fs, respectively. The initial position of the front of the foil is at $x = 50$ μm and its thickness is 2 μm. The laser pulse impinges on the foil front at $t = 167$ fs.

We now consider the evolution of the laser pulse and the longitudinal electrostatic field in more detail. Figure 2a shows that at $t = 240$ fs the laser field is limited to a narrow region near the front surface of the foil and a solitary wave is formed. Large space-charge electrostatic fields at the front and back sides of the foil are induced by the laser-expelled electrons. Multiple hot-electron recirculation contributes to the heating of the foil. Figure 2b shows that when the solitary wave begins to evolve into a CES, the space-charge field in the expanding plasma has significantly increased (up to 29 TV/m). As the electron plasma continues to expand, the relativistic mass increase lowers the plasma frequency $\omega_p \propto \sqrt{n_e/\langle\gamma\rangle}$, where $\langle\gamma\rangle$ is the cycle averaged relativistic factor. The skin depth becomes comparable to the thickness of the electron layer, so that the laser pulse can transmit through the plasma, i.e., SIT occurs in the overdense plasma (Lefebvre & Bonnaud, 1995). The critical field strength is given by (Kaw & Dawson, 1970)

$$a_0 = \begin{cases} \sqrt{(n_e/n_c)^2 - 1} & \text{for circular polarization,} \\ 4n_e/\pi n_c & \text{for linear polarization.} \end{cases} \quad (4)$$

The initial plasma density in the cases studied here is $n_e = 10n_c$. According to Eq. (4), the threshold field for the transition is $a_0 = 12.7$, which is lower than the laser strength $a_0 = 16$. Figure 2c shows that the laser pulse can transmit through the plasma because of SIT. In view of Figures 1b and 1c, we see that the laser-driven CES continuously reflects and thus accelerates the upstream ions.

The transmitting laser pulse can also expel a significant number of the target-interior electrons out of the plasma foil. The increase in the electron number in the rear vacuum region in turn enhances the sheath field. The electron phase space and the space-charge field at $t = 350$ fs and 400 fs are shown in Figure 3. We see that a hot-electron bunch is generated by the ponderomotive force of the propagating laser pulse, whose front profile is considerably steepened by the laser-plasma interaction that leads to the SIT, as can be seen in Figure 2c.

At the same time, the electrons behind the foil are pulled out and pushed back into the foil by the 2ω-oscillating component of the ponderomotive force. However, the more energetic electrons cannot return to the foil because of their high forward momentum and they remain outside, forming a second hot-electron bunch in the rear vacuum, behind the electrons from the front target surface. The two hot-electron bunches co-moving with the propagating laser pulse can efficiently enhance the target-backside sheath field by increasing its intensity as well as its spatial extent. It follows that the ions in the sheath can be accelerated more strongly and over a longer distance.

We now consider in more detail the dynamics of the CESA and TNSA ions. Figure 4 shows the evolution of the

https://doi.org/10.1017/S0263034609000433 Published online by Cambridge University Press

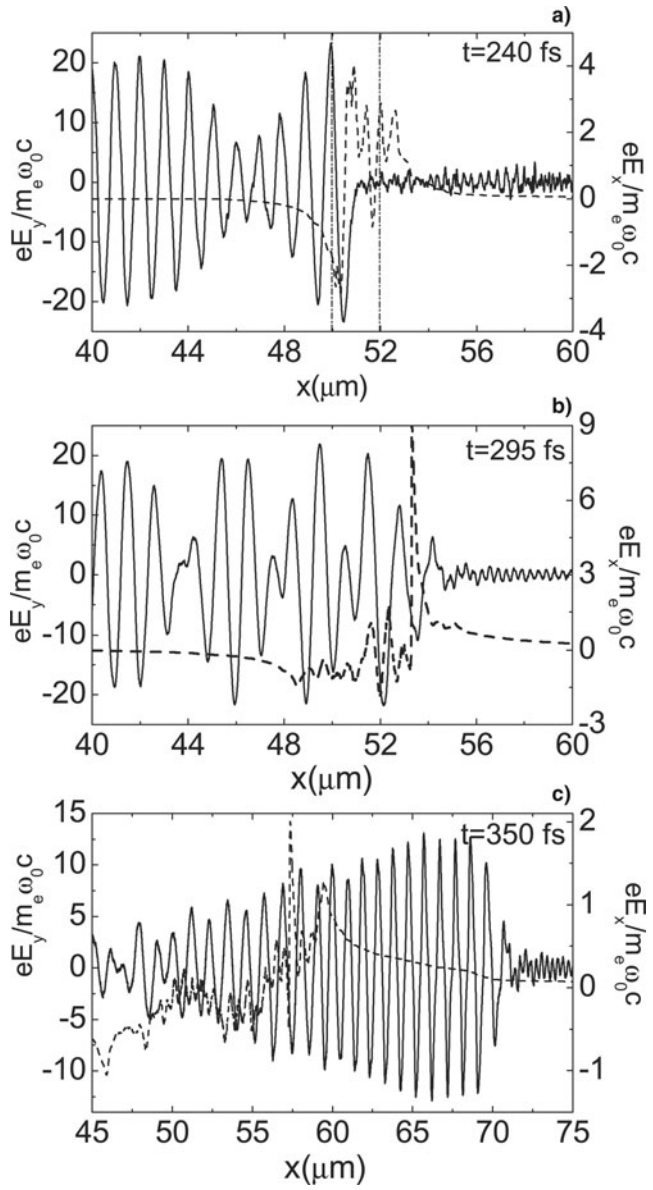

Fig. 2. The longitudinal (dashed line) and transverse (solid line) electric fields at (**a**) $t = 240$ fs, (**b**) $t = 295$ fs, and (**c**) $t = 350$ fs. The dash-dot line in Figure 2a indicates the initial edges of the foil.

electrostatic field E_x experienced by typical CESA and TNSA ions and their energy gain. One can see that the quasi-static electric field E_x experienced by the CESA ion initially increases and reaches a peak at about $t = 285$ fs, when the ion is at the peak of the solitary wave. At that moment, the ion in the frame moving with the soliton experiences a decelerating E_x. However, the soliton rapidly (in $\sim$5 fs) evolves into a CES. If the velocity $-v_i$ of the ion in the shock frame satisfies $m_i v_i^2/2 < e\lambda_D E_x$, where $E_x \sim k_B T_e/e\lambda_D$ is the CES amplitude and $\lambda_D = \sqrt{k_B T_e/4\pi n_e e^2}$ is the Debye length of the hot electrons, the ion will be reflected with the velocity $v_{\rm shock} + v_i$ in the laboratory frame. Such CESA ions will overtake the shock wave due to their higher speed. Thus they experience the CES again at a higher

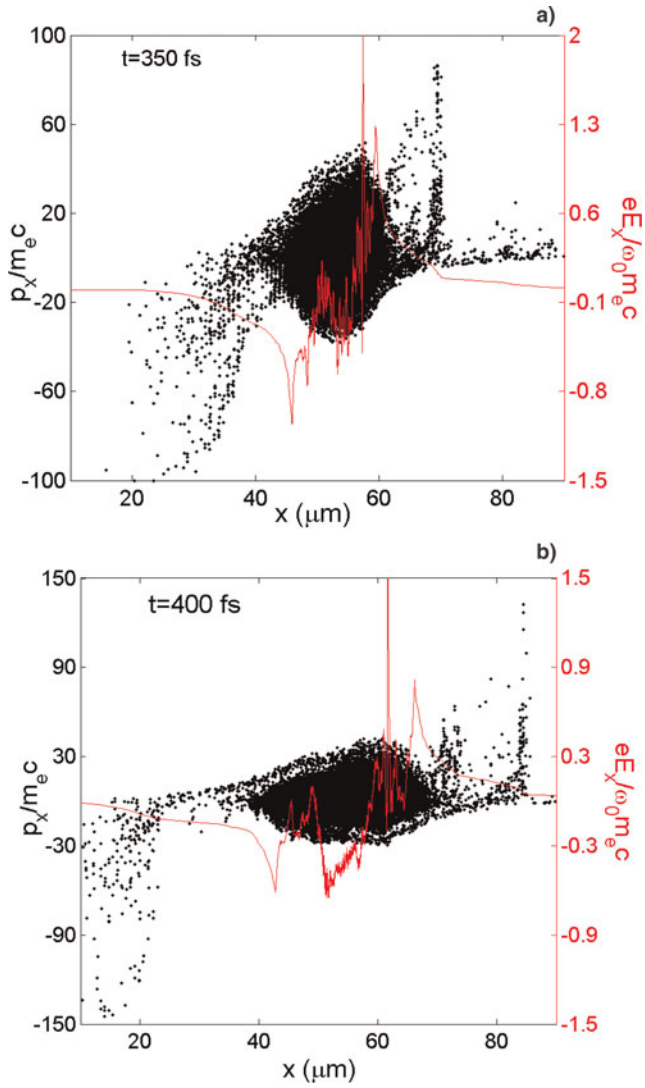

Fig. 3. (Color online) Electron phase space (x, p_x) (black) and longitudinal electric field (red) at (**a**) $t = 350$ fs and (**b**) $t = 400$ fs.

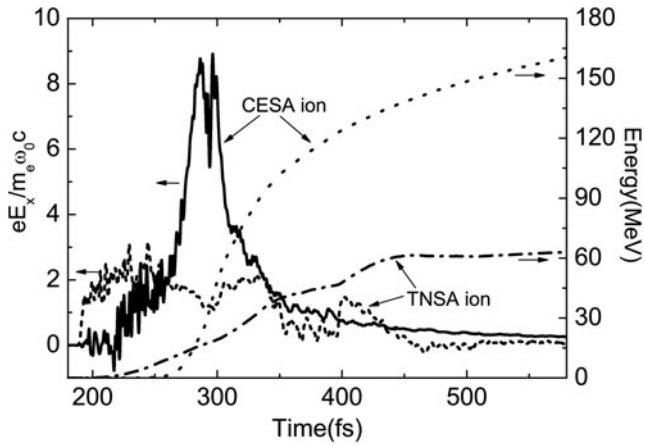

Fig. 4. The longitudinal field E_x experienced by a typical CESA ion (solid line) and the ion energy (dotted line) as functions of time. The dash and the dash-dot lines represent the longitudinal field experienced by a typical TNSA ion and its energy, respectively.

https://doi.org/10.1017/S0263034609000433 Published online by Cambridge University Press

field level and are further accelerated, and the process is repeated. At $t = 340$ fs these ions eventually overtake the TNSA ions, which have been experiencing a nearly constant sheath field $eE_x/m\omega_0 c \sim 2$. However, after being overtaken by the CESA ions, the TNSA ions become shielded by the latter from the sheath field. In fact, one can see that after $t \sim 450$ fs the energy of the typical TNSA ion becomes constant at 63.5 MeV. In contrast, the typical CESA ion is further accelerated by the sheath field of the hot electrons driven by the transmitted laser pulse. Its energy can reach 160 MeV, which is more than twice that of the typical TNSA-accelerated ion.

OPAQUE TARGET

For comparison, we have also considered the case in which the plasma foil is completely opaque to the laser pulse. Opaqueness is realized by using a higher plasma density, here $n_0 = 20\,n_c$. The other simulation parameters are the same as that for Fig. 1. According to Eq. (4), the SIT threshold for this density is $a_0 = 25$, which is much larger than the $a_0 = 16$ used in the simulation. Thus, the laser cannot propagate in the plasma. Instead, it launches in the front region of the foil a CES whose velocity is only $0.05\,c$ (but its Mach number is still larger than the critical value since the foil electrons are not efficiently heated) because of the high plasma density. Figure 5a shows the ion phase space at $t = 240$ fs. One can see that a CES is formed inside the front part of the target. The ions at the right are due to TNSA of the target-backsurface ions.

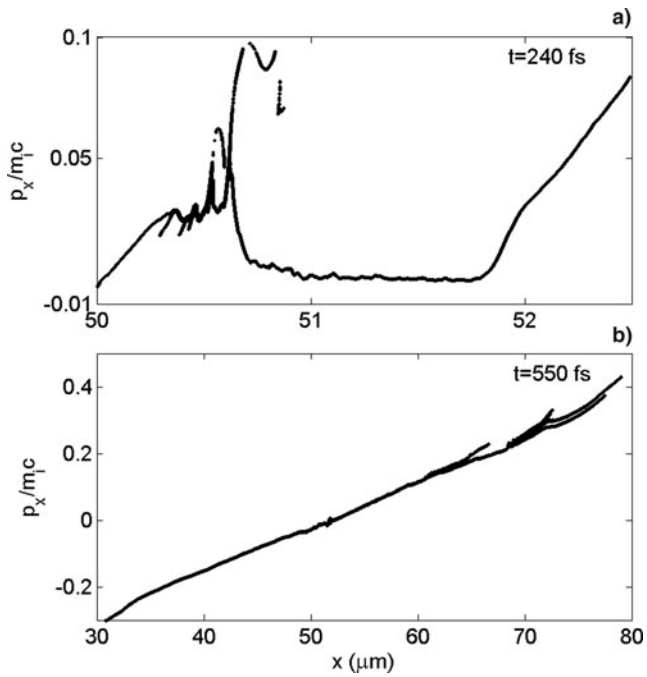

Fig. 5. Ion phase space (x, p_x) at (**a**) $t = 240$ fs and (**b**) $t = 550$ fs. Here, the foil density is $n_{e0} = 20n_c$ and it is opaque to the laser. The other parameters are the same as in Figure 1.

Again, a typical CESA ion will be further accelerated in the sheath field (see Figure 5b) and its velocity will be larger than the velocity of the TNSA ions, agreeing with the results of Silva *et al.* (2004). The maximum velocity of the TNSA ion at $t = 550$ fs is $0.35\,c$, which is nearly the same at that for the $n_0 = 10\,n_c$ case at the same instant. This similarity can be expected since TNSA (of the foil-backside ions) should be independent of the foil density. However, the maximum speed of the CESA ion is only $0.395\,c$, which is far lower than that of the $n_0 = 10\,n_c$ case. In fact, the corresponding ion energy is only 82 MeV, about half of that (156 MeV) of the $n_0 = 10\,n_c$ case at the same instant. This result is also expected, since the opaque target case the laser pulse, being stopped, absorbed, and reflected at the target front, it cannot continuously accelerate and expel the target-interior electrons to enhance the plasma expansion and the backside sheath field. Therefore, we can conclude that CESA of ions in the presence of SIT is superior to TNSA and CESA in a opaque foil.

CONCLUSION

In this article, the interaction of a laser pulse with a thin foil is studied using one-dimensional PIC simulation. It is shown that for the chosen laser and foil parameters, a CES can be generated and it can continuously reflect the upstreaming ions to high energies in the expanding plasma, when the plasma foil becomes transparent to the laser pulse due to SIT. The propagating laser pulse expels not only the foil-front electrons but also the electrons in the foil interior. Two hot-electron groups are thus generated and transported to the foil backside, producing an enhanced and spatially extended sheath field. As they reach the sheath, the CESA ions are further accelerated by the latter and they can overtake the TNSA ions. The latter are then shielded by the CESA ions, which can eventually attain energies much higher than that of the TNSA ions.

It should be pointed out that the energy spectrum of the ions first accelerated by the CES and then by the sheath field over a long distance in the expanding plasma is, as expected, rather broad. How to obtain quasi-monoenergetic ions from CESA remains to be investigated. Nevertheless, the results here should be useful to future theoretical and experimental investigations on shock acceleration of ions in laser-plasma interaction and their applications.

ACKNOWLEDGMENTS

This work was supported by the National Natural Science Foundation of China (NNSFC) under the grant Nos. 10875015, 10725521, 10834008, 10835003, and partially by the National Basic Research Program of China (973) under the grant Nos. 2006CB806004 and 2007CB815103. BSX is also supported by the New Century Excellent Talents in University of China. The authors would like to thank Dr. Hongyu Wang for his

https://doi.org/10.1017/S0263034609000433 Published online by Cambridge University Press

contribution to computational technique. The numerical simulations were performed at the HSCC of the Beijing Normal University.

REFERENCES

Badziak, J., Gãlowacz, S., Jabãloński, S., Parys, P., Wołowski, J. & Hora, H. (2005). Laser-driven generation of high-current ion beams using skin-layer ponderomotive acceleration. *Laser Part. Beams* **23**, 401–409.

Brambrink, E., Roth, M., Blazevic, A. & Schlegel, T. (2006). Modeling of the electrostatic sheath shape on the rear target surface in short-pulse laser-driven proton acceleration. *Laser Part. Beams* **24**, 163–168.

Chen, M., Sheng, Z.M., Dong, Q.L., He, M.Q., Li, Y.T., Bari, M.A. & Zhang, J. (2007). Collisionless electrostatic shock generation and ion acceleration by ultraintense laser pulses in overdense plasmas. *Phys. Plasmas* **14**, 053102.

Cowan, T.E., Fuchs, J., Ruhl, H., Kemp, A., Audebert, P., Roth, M., Stephens, R., Barton, I., Blazevic, A., Brambrink, E., Cobble, J., Fernández, J., Gauthier, J.C., Geissel, M., Hegelich, M., Kaae, J., Karsch, S., Lesage, G.P., Letzring, S., Manclossi, M., Meyroneinc, S., Newkirk, A., Pépin, H. & Renard-Legalloudec, N. (2004). Ultralow Emittance, Multi-MeV Proton Beams from a Laser Virtual-Cathode Plasma Accelerator. *Phys. Rev. Lett.* **92**, 204801.

Denavit, J. (1992). Absorption of high-intensity subpicosecond lasers on solid density targets. *Phys. Rev. Lett*. **69**, 3052.

Desai, T., Dezulian, R. & Batani, D. (2007). Radiation e®ects on shock propagation in Al target relevant to equation of state measurements. *Laser Part. Beams* **25**, 23–30.

D'humières, E., Lefebvre, E., Gremillet, L. & Malka, V. (2005). Proton acceleration mechanisms in high-intensity laser interaction with thin foils. *Phys. Plasmas* **12**, 062704.

Eliezer, S., Murakaml, M. & Val, J.M.M. (2007). Equation of state and optimum compression in inertial fusion energy. *Laser Part. Beams* **25**, 585–592.

Flippo, K., Hegelich, B.M., Albright, B.J., Yin, L., Gautier, D.C., Letzring, S., Schollmeier, M., Schreiber, J., Schulze, R. & Fernandez, J.C. (2007). Laser-driven ion accelerators: Spectral control, monoenergetic ions and new acceleration mechanisms. *Laser Part. Beams* **25**, 3–8.

Forslund, D.W. & Shonk, C.R. (1970). Formation and structure of electrostatic collisionless shock. *Phys. Rev. Lett*. **25**, 1699–1702.

Forslund, D.W. & Freidberg, J.P. (1971). Theory of laminar collisionless shocks. *Phys. Rev. Lett*. **27**, 1189–1192.

He, M.Q., Dong, Q.L., Sheng, Z.M., Weng, S.M., Chen, M., Wu, H.C. & Zhang, J. (2007). Acceleration dynamics of ions in shocks and solitary waves driven by intense laser pulses. *Phys. Rev. E*. **76**, 035402.

Hora, H. (2007). New aspects for fusion energy using inertial coñnement. *Laser Part. Beams* **25**, 37–45.

Huang, Y., Lan, X., Duan, X., Tan, Z., Wang, N., Shi, Y., Tang, X. & He, Y. (2007). Hot-electron recirculation in ultraintense laser pulse interactions with thin foils. *Phys. Plasmas* **14**, 103106.

Huang, Y., Duan, X., Lan, X., Tan, Z., Wang, N., Tang, X. & He, Y. (2008). Time-dependent neutral-plasma isothermal expansions into a vacuum. *Laser Part. Beams* **26**, 671–675.

Kaw, P. & Dawson, J. (1970). Relativistic nonlinear propagation of laser beams in cold overdense plasmas. *Phys. Fluids* **13**, 472–481.

Kruer, W.L. & Estabrook, K. (1985). $J \pounds B$ heating by very intense laser light. *Phys. Fluids* **28**, 430–432.

Lebo, I.G., Lebo, A.I., Batani, D., Dezulian, R., Benocci, R., Jafer, R. & Krousky, E. (2008). Simulations of shock generation and propagation in laser-plasmas. *Laser Part. Beams* **26**, 179C188.

Lefebvre, E. & Bonnaud, G. (1995). Transparency/Opacity of a solid target illuminated by an ultrahigh-intensity laser pulse. *Phys. Rev. Lett*. **74**, 2002–2005.

Limpouch, J., Psikal, J., Andreev, A.A., Platonov, K.Yu. & Kawata, S. (2008). Enhanced laser ion acceleration from mass-limited targets. *Laser Part. Beams* **26**, 225C234.

Liu, M.P., Wu, H.C., Xie, B.S., Liu, J., Wang, H.Y. & Yu, M.Y. (2008). Energetic collimated ion bunch generation from an ultraintense laser interacting with thin concave targets. *Phys. Plasmas* **15**, 063104.

Mackinnon, A.J., Sentoku, Y., Patel, P.K., Price, D.W., Hatchett, S., Key, M.H., Andersen, C., Snavely, R. & Freeman, R.R. (2002). Enhancement of proton acceleration by hot-electron recirculation in thin foils irradiated by ultraintense laser pulses. *Phys. Rev. Lett*. **88**, 215006.

Mackinnon, A.J., Patel, P.K., Borghesi, M., Clarke, R.C., Freeman, R.R., Habara, H., Hatchett, S.P., Hey, D., Hicks, D.G., Kar, S., Key, M.H., King, J.A., Lancaster, K., Neely, D., Nikkro, A., Norreys, P.A., Notley, M.M., Phillips, T.W., Romagnani, L., Snavely, R.A., Stephens, R.B. & Town, R.P.J. (2006). Proton radiography of a laser-driven implosion. *Phys. Rev. Lett*. **97**, 045001.

Mckenna, P., Carroll, D.C., Lundh, O., Näurnberg, F., Markey, K., Bandyopadhyay, S., Batani, D., Evans, R.G., Jafer, R., Kar, S., Neely, D., Pepler, D., Quinn, M.N., Redaelli, R., Roth, M., Wahlsträom, C.-G., Yuan, X.H. & Zepf, M. (2008). E®ects of front surface plasma expansion on proton acceleration in ultraintense laser irradiation of foil targets. *Laser Part. Beams* **26**, 591–596.

Nickles, P.V., Ter-Avetisyan, S., Schnäuerer, M., Sokollik, T., Sandner, W., Schreiber, J., Hilscher, D., Jahnke, U., Andreev, A. & Tikhonchuk, V. (2007). Review of ultrafast ion acceleration experiments in laser plasma at Max Born Institute. *Laser Part. Beams* **25**, 347–363.

Nieter, C. & Cray, J.R. (2004). VORPAL: a versatile plasma simulation code. *J. Comput. Phys*. **196**, 448–473.

Romagnani, L., Bulanov, S.V., Borghesi, M., Audebert, P., Gauthier, J.C., Läowenbräuck, K., Mackinnon, A.J., Patel, P., Pretzler, G., Toncian, T. & Willi, O. (2008). Observation of collisionless shocks in laser-plasma experiments. *Phys. Rev. Lett*. **101**, 025004.

Roth, M., Cowan, T.E., Key, M.H., Hatchett, S.P., Brown, C., Fountain, W., Johnson, J., Pennington, D.M., Snavely, R.A., Wilks, S.C., Yasuike, K., Ruhl, H., Pegoraro, F., Bulanov, S.V., Campbell, E.M., Perry, M.D. & Powell, H. (2001). Fast ignition by intense laser-accelerated proton beams. *Phys. Rev. Lett*. **86**, 436–439.

Roth, M., Brambrink, E., Audebert, P., Blazevic, A., Clarke, R., Cobble, J., Cowan, T.E., Fernandez, J., Fuchs, J., Geissel, M., Habs, D., Hegelich, M., Karsch, S., Ledingham, K., Neely, D., Ruhl, H., Schlegel, T. & Schreiber, J. (2005). Laser accelerated ions and electron transport in ultra-intense laser matter interaction. *Laser Part. Beams* **23**, 95–100.

https://doi.org/10.1017/S0263034609000433 Published online by Cambridge University Press

Santala, M.I.K., Zepf, M., Beg, F.N., Clark, E.L., Dangor, A.E., Krushelnick, K., Tatarakis, M., Watts, I., Ledingham, K.W.D., Mccanny, T., Spengcer, I., Machacek, A.C., Allott, R., Clarke, R.J. & Norreys, P.A. (2001). Production of radioactive nuclides by energetic protons generated from intense laser-plasma interactions. *Appl. Phys. Lett*. **78**, 19–21.

Silva, L.O., Marti, M., Davies, J.R., Fonseca, R.A., Ren, C., Tsung, F.S. & Mori, W.B. (2004). Proton shock acceleration in laser-plasma interactions. *Phys. Rev. Lett*. **92**, 015002.

Snavely, R.A., Key, M.H., Hatchett, S.P., Cowan, T.E., Roth, M., Phillips, T.W., Stoyer, M.A., Henry, E.A., Sangster, T.C., Singh, M.S., Wilks, S.C., Mackinnon, A., Offenberger, A., Pennington, D.M., Yasuike, K., Langdon, A.B., Lasinski, B.F., Johnson, J., Perry, M.D. & Campbell, E.M. (2000). Intense high-energy proton beams from petawatt-laser irradiation of solids. *Phys. Rev. Lett*. **85**, 2945–2948.

Sorasio, G., Marti, M., Fonseca, R. & Silva, L.O. (2006). Very high mach-number electrostatic shocks in collisionless plasmas. *Phys. Rev. Lett*. **96**, 045005.

Wei, M.S., Manglez, S.P.D., Najmudin, Z., Walton, B., Gopal, A., Tatarakis, M., Dangor, A.E., Clark, E.L., Evans, R.G., Fritzler, S., Clarke, R.J., Hernandez-Gomez, C., Neely, D., Mori, W., Tzoufras, M. & Krushelnick, K. (2004). Ion acceleration by collisionless shocks in high-intensity-laser Cunderdense-plasma interaction. *Phys. Rev. Lett*. **93**, 155003.

Winterberg, F. (2008). Lasers for inertial confinement fusion driven by high explosives. *Laser Part. Beams* **26**, 127–135.

Yin, L., Albright, B.J., Hegelich, B.M. & Fernandez, J.C. (2006). GeV laser ion acceleration from ultrathin targets: The laser break-out afterburner. *Laser Part. Beams* **24**, 291–298.

Zhidkov, A., Uesaka, M., Sasaki, A. & Daido, H. (2002). Ion acceleration in a solitary wave by an intense picosecond laser pulse. *Phys. Rev. Lett*. **89**, 215002.

https://doi.org/10.1017/S0263034609000433 Published online by Cambridge University Press